Analysis of the Point-Diffraction Interferometer and Application to Testing of Pressure-Loaded Windows

Merle E. Riley, Edward L. Patterson

MASTER

Sandia National Laboratories

2900-Q(3-80)

DISCLAIMER

This report was prepared as an account of work sponsored by an agency of the United States Government. Neither the United States Government nor any agency Thereof, nor any of their employees, makes any warranty, express or implied, or assumes any legal liability or responsibility for the accuracy, completeness, or usefulness of any information, apparatus, product, or process disclosed, or represents that its use would not infringe privately owned rights. Reference herein to any specific commercial product, process, or service by trade name, trademark, manufacturer, or otherwise does not necessarily constitute or imply its endorsement, recommendation, or favoring by the United States Government or any agency thereof. The views and opinions of authors expressed herein do not necessarily state or reflect those of the United States Government or any agency thereof.

DISCLAIMER

Portions of this document may be illegible in electronic image products. Images are produced from the best available original document.

PAGES __1__ to __2__

WERE INTENTIONALLY

LEFT BLANK

ANALYSIS OF THE POINT-DIFFRACTION INTERFEROMETER AND

APPLICATION TO TESTING OF PRESSURE-LOADED WINDOWS

Merle E. Riley and Edward L. Patterson
Sandia National Laboratories
Albuquerque, New Mexico 87185

ABSTRACT

A diffraction-theory analysis is given of the point-diffraction interferometer. The leading error present in the reference beam is expressed as a function of the pinhole diameter. A second part of the work presents a ray-tracing analysis of pressure-loaded windows; the leading-order distortion for incident plane waves is a weak lensing. The point-diffraction interferometer is used to confirm the analysis for an astigmatic aberration produced by cylindrical deformation of a plastic window.

DISTRIBUTION OF THIS DOCUMENT IS UNLIMITED

3-4

TABLE OF CONTENTS

FIGURE CAPTIONS

Fig. 1. Schematic drawing of the PDI arrangement used in the theoretical analysis of Section II.A........................ 9

Fig. 2. PDI interferogram showing defocus which corresponds to Eq. (6) of the text having a nonzero δ_z and $\delta_x = \delta_y = 0$.... 22

Fig. 3. PDI interferogram with $\delta_x = \delta_y = \delta_z = 0$ and relatively good input beam. This is a null position with all-bright uniform field.. 22

Fig. 4. PDI interferogram with nonzero δ_x or δ_y and $\delta_z = 0$. This is finite tilt with a reference beam phase given by Eq. (6).... 23

Fig. 5. PDI interferogram exhibiting almost pure astigmatism in the input beam. This photo reveals an input beam error and not an adjustment of the interferometer as in Figs. 2, 3, and 4.. 23

Fig. 6. PDI interferogram with much too large of a w_p/w_{spot} ratio. This exhibits a severe reference beam error.............. 25

Fig. 7. Ray-tracing diagram used in the theoretical development in Section III for bent windows........................... 27

Fig. 8. PDI interferogram of plastic sheet. The sheet is unbent and contains a few waves of nonuniformity in thickness..... 35

Fig. 9. PDI interferogram of bent plastic sheet. The center of curvature is off-center in the photo aperture. A two-centimeter scale is indicated below the figure. Discussion is present near the end of Section III.......... 35

I. Introduction

The point-diffraction interferometer[1,2] (PDI) is a new type of instrument which possesses certain advantages for analyzing optical-beam phase fronts. First of all, it is a common path instrument and very insensitive to vibration. Second, it is very compact and may be inserted into an optical chain with very little disruption. Third, it is a standard interferometer as opposed to a shearing interferometer because the test beam is compared to a high-quality beam; consequently, the interferograms are subject to standard interpretation.

The primary purpose of this work is to analyze the interferometer itself to determine the limitations imposed by diffraction theory on the quality of the reference beam. With this accomplished, one can be confident that the diagnosis of the test beam is reliable. A second purpose is to use the instrument to verify a theoretical prediction about the optical properties of windows deformed by pressure loading.

Section II gives the diffraction theory of PDI operation and illustrates the performance of the laboratory instrument in hand. Section III gives a theoretical analysis of loaded windows and shows how the PDI may be used to detect the phase front error.

II. Theory of PDI Operation and Testing

A standard interferometer works by combining (interfering) a light beam of unknown quality with a beam of reference quality. We note that the "analysis" of a beam is synomynous with analysis of an optical element present in the beam. The PDI is unique among interferometers in that it uses as a reference beam a "point" source of light generated by the beam being tested. The point source is really a small aperture, a pinhole of micron size, and questions immediately arise as to the quality of a reference beam generated by a pinhole whose diameter is of the magnitude

of the diffraction spot size of the light beam and focusing system. Section II.A. gives a theoretical analysis of the reference beam's quality and Section II.B. presents some experimental illustrations as well as verifications of the theoretical analysis by reference to some new data available in the literature.

II.A. Theoretical Analysis of the PDI

Figure 1 gives a schematic picture of a typical PDI configuration. A beam of light enters from the left and is focused down by the first lens onto a transparent substrate covered with a partially-transmitting thin-film filter containing a pinhole. The pinhole generates a diffracted beam which interferes with the portion of the input beam transmitted through the filter.

Let $0'''$, $0''$, $0'$, and 0 denote origins of Cartesian coordinate systems erected along the optic z-axis at .the first lens, the pinhole plane, the second lens, and the image plane. The second lens serves as a relay for the beam from some upstream plane to the final image on the observation plane. The example of Fig. 1 relays the first-lens plane to the image plane with unit magnification and inversion. This example is used in the rest of the theoretical analysis; the only requirement in general is that the image plane be conjugate to the particular plane being examined. If the beam aberrations which result from the testable defects have a Rayleigh range[3] long enough to be visible away from the test plane, it is not necessary to relay the test plane at all: the second lens may be omitted and the same interferogram may be obtained anywhere downstream of the near-field region of the pinhole but within the Rayleigh range of the aberrations.

Let the coordinates of the pinhole center be δ_x, δ_y, δ_z relative to
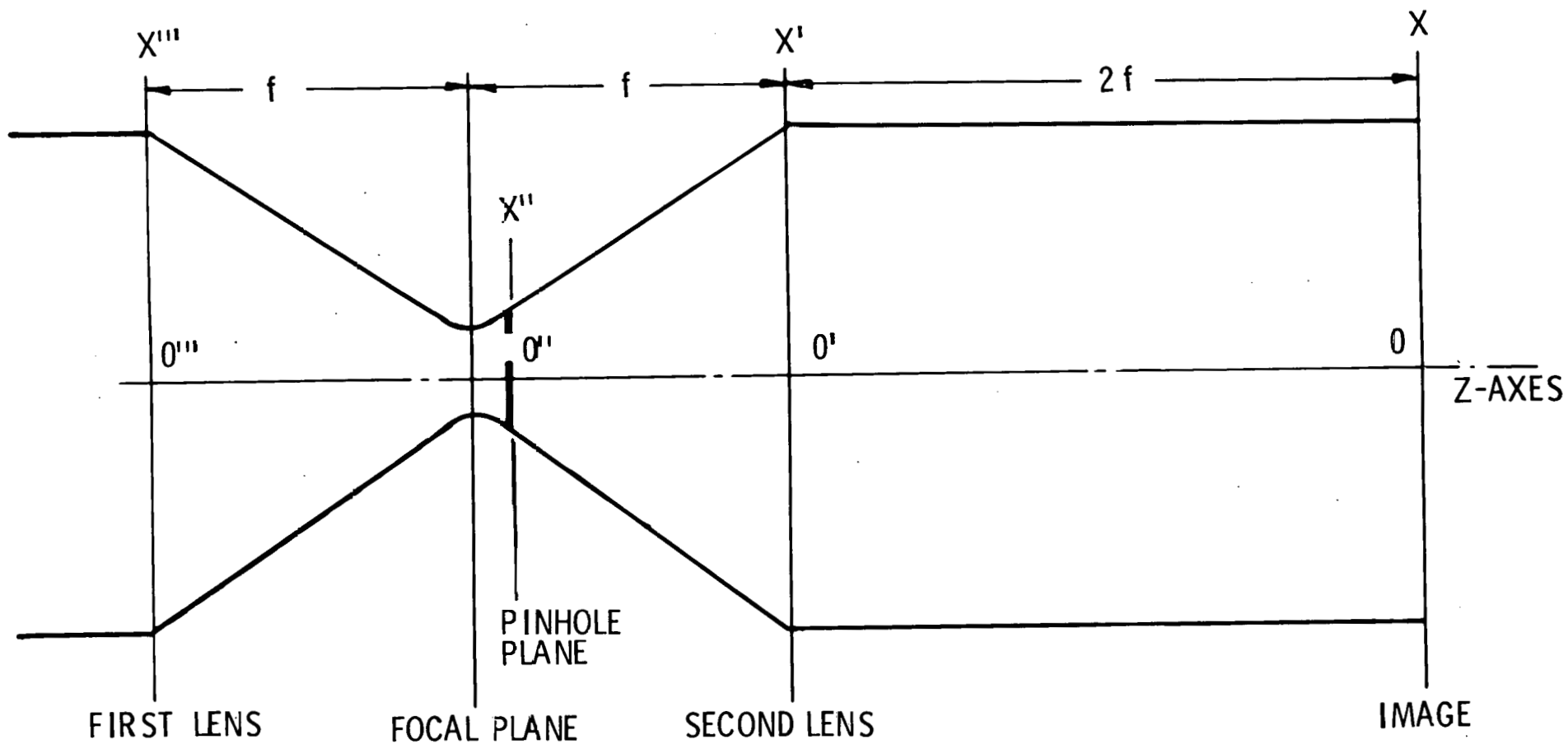
Fig. 1.   Schematic drawing of the PDI arrangement used
in the theoretical analysis of Section II.A.

the paraxial focus of the first lens. The transverse components of the coordinate systems are denoted by a two-component vector, $\vec{r} = x\hat{e}_x + y\hat{e}_y$. The $0'''$, $0''$, $0'$ and 0 coordinates are related by simple translations along the optic z-axis:

$$\vec{r}''' = \vec{r}'' = \vec{r}' = \vec{r}$$

$$z''' = z'' + f + \delta_z$$

$$z'' = z' + f - \delta_z$$

$$z' = z + 2f \ .$$

Paraxial propagation[4] may be written in any of the coordinate systems:

$$\vec{E} \approx \hat{e}_\lambda E_\lambda = \hat{e}_\lambda \mathcal{E}_z(\vec{r}) e^{-ikz}$$

$$\nabla_r^2 \mathcal{E}_z(\vec{r}) - 2ik \frac{\partial}{\partial z} \mathcal{E}_z(\vec{r}) = 0$$

$$\mathcal{E}_{z+L}(\vec{r}) = \int d^2r' K_L(\vec{r} - \vec{r}') \mathcal{E}_z(\vec{r}')$$

$$K_L(\vec{r} - \vec{r}') = \frac{ik}{2\pi L} e^{-i \frac{k}{2L} |\vec{r} - \vec{r}'|^2} \ .$$

The electrical amplitude is needed at four of the planes designated in Fig. 1; these are $\mathcal{E}_{input}$, $\mathcal{E}_{pinhole}$, $\mathcal{E}_{L2}$, and $\mathcal{E}_{image}$. The amplitude transmitted through the filter and pinhole aperture may be approximated as the incident amplitude, $\mathcal{E}_{pinhole}$, times a transmission factor,[2] $t = t(\vec{r}'')$:

$$t = W + \tau(1 - W)$$

$$= \tau + (1 - \tau)W$$

$$\approx \tau + W \ .$$

$\tau^* \tau = T$ is the background transmission of the filter and $W = W(\vec{r}'')$ is a

weighting function which gives the transmission profile of the pinhole aperture. Let $\vec{\delta} = \delta_x \hat{e}_x + \delta_y \hat{e}_y$ be the transverse location of the pinhole and let $\vec{r}_p = \vec{r}'' - \vec{\delta}$ with $r_p = |\vec{r}_p|$; then a circular pinhole of soft aperture might be represented by

$$W = W(r_p) = e^{-(r_p/w_p)^2} ,$$

but the more appropriate hard-apertured pinhole is best described by

$$W = W(r_p) = 1 - \theta(r_p - w_p) ,$$

where w_p is the radius and θ is the unit step function. The emerging beam is a superposition of two beams: one is an unapertured beam simply reduced by the constant τ; the other is diffracted by the transverse limitation imposed by W. The form of $t(\vec{r}'')$ makes this clear.

The first step in the analysis requires evaluation of the field incident on the pinhole plane:

$$\mathcal{E}_{pinhole}(\vec{r}'') = \int d^2 r''' K_{f+\delta_z}(\vec{r}'' - \vec{r}''')e^{i\frac{k}{2f}r'''^2} \mathcal{E}_{input}(\vec{r}''') . \qquad (1)$$

The exponential factor under the integral accounts for the focusing by the first lens. The second step is to modify $\mathcal{E}_{pinhole}$ by the transmission factor and to propagate the beam to the second lens:

$$\mathcal{E}_{L2}(\vec{r}') = \int d^2 r'' K_{f-\delta_z}(\vec{r}' - \vec{r}'')t(\vec{r}'')\mathcal{E}_{pinhole}(\vec{r}'') .$$

Since t can be written as the sum, $\tau + W$, $\mathcal{E}_{L2}$ is calculated as the sum of two beams, $\mathcal{E}_{L2}^{ref}$ and $\mathcal{E}_{L2}^{trans}$:

$$\mathcal{E}_{L2}^{trans}(\vec{r}') = \tau \int d^2 r'' K_{f-\delta_z}(\vec{r}' - \vec{r}'')\mathcal{E}_{pinhole}(\vec{r}'')$$

$$\mathcal{E}_{L2}^{ref}(\vec{r}') = \int d^2 r'' K_{f-\delta_z}(\vec{r}' - \vec{r}'')W\mathcal{E}_{pinhole}(\vec{r}'') .$$

11

The final step is to evaluate the image-plane fields by propagating both

these beams a distance of 2f, after lensing by L2:

$$\mathcal{E}_{image}(\vec{r}) = \int d^2r' K_{2f}(\vec{r} - \vec{r}')e^{i\frac{k}{2f}r'^2} \mathcal{E}_{L2}(\vec{r}')$$

$$\mathcal{E}_{image} = \mathcal{E}_{image}^{ref} + \mathcal{E}_{image}^{trans} .$$

$\mathcal{E}_{image}^{trans}$ may be evaluated directly by making use of the imaging property

of lens L2:

$$\mathcal{E}_{image}^{trans}(\vec{r}) = \int d^2r' K_{2f}(\vec{r} - \vec{r}')e^{i\frac{k}{2f}r'^2} \tau$$

$$\times \int d^2r'' K_{f-\delta_z}(\vec{r}' - \vec{r}'') \int d^2r''' K_{f+\delta_z}(\vec{r}'' - \vec{r}''')e^{i\frac{k}{2f}r'''^2} \mathcal{E}_{input}(\vec{r}''')$$

$$= \tau \int d^2r' K_{2f}(\vec{r} - \vec{r}')e^{i\frac{k}{2f}r'^2}$$

$$\times \int d^2r''' K_{2f}(\vec{r}' - \vec{r}''')e^{i\frac{k}{2f}r'''^2} \mathcal{E}_{input}(\vec{r}''')$$

$$= -\tau \int d^2r' K_{2f}(\vec{r} - \vec{r}')$$

$$\times \int d^2r''' K_{-2f}(\vec{r}' + \vec{r}''')\mathcal{E}_{input}(\vec{r}''')$$

$$= -\tau \int d^2r''' K_0(\vec{r} + \vec{r}''')\mathcal{E}_{input}(\vec{r}''') ,$$

or,

$$\mathcal{E}_{image}^{trans}(\vec{r}) = -\tau\mathcal{E}_{input}(-\vec{r}) .$$

12

The following properties of the propagator were used to demonstrate the imaging:

$$\int d^2r' K_{L_1}(\vec{r} - \vec{r}') K_{L_2}(\vec{r}' - \vec{r}'') = K_{L_1+L_2}(\vec{r} - \vec{r}'')$$

$$K_0(\vec{r} - \vec{r}') = \delta^2(\vec{r} - \vec{r}') .$$

This completes the determination of the "transmitted" portion of the beam which contains the information relevant to the phase distortion present in the input beam. The second part of this step in the analysis is to determine the quality of the "reference" portion of the beam.

The reference beam at the image plane is easily expressed in terms of the amplitude incident on the pinhole, $\delta_{pinhole}$:

$$\delta_{image}^{ref}(\vec{r}) = \int d^2r' K_{2f}(\vec{r} - \vec{r}') e^{ikr'^2/2f}$$

$$\times \int d^2r'' K_{f-\delta_z}(\vec{r}' - \vec{r}'') W(\vec{r}'') \delta_{pinhole}(\vec{r}'') \qquad (2)$$

$$= -e^{-ikr^2/2f} \int d^2r'' K_{-f-\delta_z}(\vec{r} + \vec{r}'') W(\vec{r}'') \delta_{pinhole}(\vec{r}'') .$$

The effective pinhole radius w_p is always assumed to be smaller than the diffraction spot size of the input beam or lens system; either

$$w_p < w_{spot}^{GB} = 2f/kw_o^{GB} = 0.32\lambda f/w_o^{GB} \qquad (3)$$

for a Gaussian TEM_{00} beam of input waist w^{GB}, or,

$$w_p < w_{spot}^{DR} = 0.61\lambda f/w_o^{HA} \qquad (4)$$

13

for a uniform input beam that is hard apertured at radius w_o^{HA} with a dark ring focal spot radius w_{spot}^{DR}. These restrictions on w_p enable simplifications to be made in the general expression for $\mathscr{E}_{image}^{ref}$ in terms of $\mathscr{E}_{pinhole}$. Under the integral in Eq. (2) the exponentials may be simplified because of the weighting of the range of integration to the pinhole region:

$$\frac{kr''^2}{2f} \leqslant \frac{kw_p^2}{2f} \leqslant \frac{kw_p}{2f} \frac{2f}{kw_o} = \frac{w_p}{wo} \ll 1 \ .$$

However,

$$\left| \frac{kxx''}{f} \right| \leqslant \frac{kw_o w_p}{f} \leqslant \frac{kw_o}{f} \frac{2f}{kw_o} = O(1) \ .$$

Combined with the stipulation that $\delta_z/f \ll 1$, all the exponentials may be simplified without introducing any restrictions on the applicability of the analysis to a typical interferometer. Thus, in terms of $\mathscr{E}_{pinhole}$:

$$\mathscr{E}_{image}^{ref}(\vec{r}) = \frac{ik}{2\pi f} e^{i\varphi_o^{ref}(\vec{r})} \int d^2r'' e^{ik\vec{r} \cdot (\vec{r}'' - \vec{\delta})f}$$

$$\text{(5)}$$

$$\times \ W(\vec{r}'')\mathscr{E}_{pinhole}(\vec{r}'') \ ,$$

where the ideal reference beam phase has been factored out,

$$\varphi_o^{ref}(\vec{r}) = \frac{k}{f} \left(-\frac{\delta_z}{2f} r^2 + \delta_x x + \delta_y y\right) \ . \tag{6}$$

$\mathscr{E}_{pinhole}$ is now expressed in terms of $\mathscr{E}_{input}$ by Eq. (1) and analogous simplifications of the exponentials are made because of the limits on the range of $\vec{r}''$. $\mathscr{E}_{input}$ is written in phase-amplitude form,

$$\mathscr{E}_{input}(\vec{r}''') = \epsilon(\vec{r}''')e^{i\psi(\vec{r}''')} \ ,$$

and $W(\vec{r}'')$ is taken to be a hard aperture of radius w_p. The final result for the combined expression of δ_{image} in terms of δ_{input} is

$$\delta_{image}^{ref}(\vec{r}) = -\frac{1}{\pi}\left(\frac{kw_p}{2f}\right)^2 e^{i\varphi_o^{ref}(\vec{r})}$$

$$\times \int d^2s \epsilon(\vec{s}) e^{i\bar{\psi}(\vec{s})} \frac{2J_1(kw_p|\vec{s}+\vec{r}|/f)}{kw_p|\vec{s}+\vec{r}|/f}$$

(7)

where we have used $\vec{s} = \vec{r}'''$ to simplify the notation and have defined

$$\bar{\psi}(\vec{s}) = \psi(\vec{s}) + \frac{k}{2f}\frac{\delta_z}{f}s^2 + \frac{k}{f}\vec{\delta}\cdot\vec{s}$$

(8)

$$= \psi(\vec{s}) - \varphi_o^{ref}(-\vec{s}) \ .$$

The integrand containing the Bessel function in Eq. (7) acts as a filtering function with the limiting property

$$\lim_{w_p \to \infty} \frac{1}{\pi}\left(\frac{kw_p}{2f}\right)^2 \frac{2J_1(x)}{x} = \delta^2(\vec{s}+\vec{r}) \ ,$$

$$x = kw_p|\vec{s}+\vec{r}|/f \ .$$

This shows $\delta_{image}^{ref}(\vec{r}) = -\delta_{input}(-\vec{r})$ if w_p is too large. In this circumstance, no interference results because of an unimproved reference beam. The properties of the function as w_p becomes small are more relevant: we define the smallness parameter α:

$$\alpha = \frac{1}{2}\left(\frac{kw_p}{2f}\right)^2 w_o^2$$

$$= \frac{1}{2}\left(\frac{w_p}{w_{spot}^{GB}}\right)^2 \qquad (9)$$

$$\approx 2\left(\frac{w_p}{w_{spot}^{DR}}\right)^2 ,$$

which measures the ratio of pinhole size to diffraction-limited spot size as defined in Eqs. (3) and (4). In terms of α and $d = |\vec{s} + \vec{r}|/w_o$ we can rewrite Eq. (7) as

$$\delta_{image}^{ref}(\vec{r}) = -\frac{2\alpha}{\pi w_o^2} e^{i\varphi_o^{ref}(\vec{r})} \int d^2s\, \epsilon(\vec{s}) e^{i\bar{\psi}(\vec{s})} F(\alpha d^2) , \qquad (10)$$

where the newly defined function F is given by

$$F(x) = J_1(2(2x)^{1/2})/(2x)^{1/2} = 1 - x + \frac{1}{3}x^2 + \cdots .$$

Phase errors in the reference beam, i.e., additions to φ_o^{ref}, arise from phase, η, of the complex integral of Eq. (10). In order to examine η we can take appropriate advantage of the presumed smallness of α to expand F in its power series. In addition, we will assume that the variation of $\bar{\psi}(\vec{s})$ over the input aperture is sufficiently small that we need to retain only the first-order, linear term in $\bar{\psi}$:

$$\eta = \tan^{-1}\left(\int d^2s \,\sin\bar{\psi}\, F \middle/ \int d^2s \,\cos\bar{\psi}\, F\right)$$

$$\approx \int d^2s \,\bar{\psi}\, F \middle/ \int d^2s\, F .$$

16

It does not matter in which order we carry out the expansions in α and $\bar{\psi}$.
We have specialized to the case where the input amplitude is constant over
the input aperture. We also set $\bar{\psi}(0) = 0$ without any loss of
generality. For convenience, we introduce a bracket notation for
the normalized area integral over the input aperture,

$$\langle x \rangle = (\pi w_o^2)^{-1} \int d^2 s \; x \; .$$

η is now expanded in powers of α:

$$\eta = \langle \bar{\psi} \rangle - \alpha(\langle d^2 \bar{\psi} \rangle - \langle d^2 \rangle \langle \bar{\psi} \rangle) + \alpha^2 \left(\frac{1}{3} (\langle d^4 \bar{\psi} \rangle - \langle d^4 \rangle \langle \bar{\psi} \rangle) \right.$$

$$\left. - \langle d^2 \rangle (\langle d^2 \bar{\psi} \rangle - \langle d^2 \rangle \langle \bar{\psi} \rangle) \right) + O(\alpha^3) \; ,$$

(11)

and various reductions are made,

$$d^2 = (s^2 + 2sru + r^2)/w_o^2 \; , \quad u = \cos(\theta_s - \theta_r) \; ,$$

$$\langle s^n \rangle = 2/(n + 2) \; , \quad \langle s^n u \rangle = 0 \; ,$$

$$\langle s^n u^2 \rangle = \frac{1}{2} \langle s^n \rangle \; .$$

The η expansion of Eq. (11) is regrouped into powers of the image plane
variable $\vec{r}$,

$$\eta = \eta_0 + \eta_1 + \eta_2 + O(\alpha^3) \; .$$

17

The first term is independent of $\vec{r}$,

$$\eta_0 = \langle \vec{\psi} \rangle - \alpha \langle (s^2 - \frac{1}{2})\vec{\psi} \rangle + \frac{1}{3}\alpha^2 \langle (s^4 - \frac{3}{2}s^2 + \frac{5}{12})\vec{\psi} \rangle \; .$$

and does not affect the reference beam phase quality. All of the s and r variables contain an implicit $1/w_0$ factor which is not written out in the expressions for η_0, η_1, and η_2. The second term is

$$\eta_1 = -2\alpha r \langle su\vec{\psi} \rangle + \alpha^2 r \langle s(\frac{4}{3}s^2 - 1)u\vec{\psi} \rangle \; ,$$

which contains only linear terms in $\vec{r}$ components that are indistinguishable from tilt adjustments of the interferometer (compare to Eq. (6)) and, consequently, are not to be treated as reference beam errors. Finally, we have

$$\eta_2 = \frac{1}{3}\alpha^2 r^2 \langle (s^2 - \frac{1}{2})\vec{\psi} \rangle + \frac{4}{3}\alpha^2 r^2 \langle s^2(u^2 - \frac{1}{2})\vec{\psi} \rangle$$

$$- \frac{2}{3}\alpha^2 r^3 \langle su\vec{\psi} \rangle$$

which contains three distinct phase corrections—defocus, astigmatism, and coma. The first of these, like the whole of η_1, is indistinguishable from an interferometer adjustment and will not be confused with any error of the input beam. The coma part of η_2 (and of η through order α^2) is

$$\eta_{coma} = -\frac{2}{3}\alpha^2 (r/w_0)^3 \frac{1}{\pi w_0^2} \int d^2 s (s/w_0)\cos(\theta_s - \theta_r)\vec{\psi}(\vec{s}) \; . \qquad (12)$$

The astigmatism of the reference beam is isolated after expanding the u^2 term:

$$\mu^2 = \cos^2(\theta_s - \theta_r) = \frac{1}{2} + \frac{1}{2}\cos(2(\theta_s - \theta_r)) ,$$

(13)

$$\eta_{astig} = \frac{2}{3}\alpha^2(r/w_o)^2 \frac{1}{\pi w_o^2} \int d^2 s (s/w_o)^2 \cos(2(\theta_s - \theta_r))\bar{\psi}(\vec{s}) .$$

We note that $\bar{\psi}$ is $\psi(\vec{s}) - \varphi_o^{ref}(-\vec{s})$ and that the φ_o^{ref} part cannot contribute to η_{astig} because of orthogonality in the angular integration. The tilt part of φ_o^{ref} does affect η_{coma} though, and one may deduce that, for each wave of tilt, one has $\alpha^2/6$ wave of coma at the maximum. It would be very satisfying if a bound could be placed on the phase error in η; we have not found any satisfactory and rigorous solution to this problem, however. One should begin the bound analysis with Eq. (10) and use the fact that one must bound the variation of η over the image plane and not the value of η. For heuristic purposes, we estimate a bound on reference beam error by using the lowest order source of error present in $\bar{\psi}$. That has been mentioned above: tilt in $\bar{\psi}$ produces coma in η. Substitution of one wave of tilt,

$$\bar{\psi} = 2\pi(s/w_o) \cos \theta_s ,$$

into Eq. (12) and evaluation of the maximum gives

$$\eta_{coma}^{max} = \frac{1}{6}\alpha^2 \bar{\psi}_{tilt}^{max} .$$

(14)

The variation in reference beam amplitude may be computed by analogous means; we have found that

$$|\delta_{image}^{ref}| \propto 1 - \alpha(r/w_o)^2 ,$$

and if we require the variation from the central maximum of the intensity to be less than 25%, Eq. (9) can be used to show

$$w_p < \frac{f}{kw_o} \quad .$$

Equations (3) and (4) now specify that the pinhole radius should be less than $w_{spot}^{GB}/2$ or $w_{spot}^{DR}/4$ in order to produce a very uniform reference beam. This analysis quantifies previous statements[1,2] about the pinhole size required for a good reference beam.

The form of the interferogram is found from $\mathcal{E}_{image}(\vec{r})$ which is in the form of a two-term complex sum, $\mathcal{E}^{ref} + \mathcal{E}^{trans}$, dropping the "image" label. Let $I = \mathcal{E}^{*}\mathcal{E}$ and decompose the terms into phase-amplitude form:

$$\mathcal{E} = |\mathcal{E}^{ref}|e^{i\varphi^{ref}} + |\mathcal{E}^{trans}|e^{i\varphi^{trans}} \quad ,$$

$$I = (|\mathcal{E}^{ref}| - |\mathcal{E}^{trans}|)^2 + |\mathcal{E}^{ref}||\mathcal{E}^{trans}|4\cos^2(\Delta/2) \quad ,$$

$$\Delta = \varphi^{trans} - \varphi^{ref} \quad .$$

Δ determines the structure of the interferogram and is the quantity of interest. The resulting interferograms may be interpreted by standard techniques. The visibility of the interferogram depends on the proper relation of τ and w_p for a given focusing system. Let $\mathcal{E}_{input} = \epsilon_o e^{i\psi}$; $\mathcal{E}_{image}^{ref}$ is given by Eq. (5) as w_p becomes small,

$$\mathcal{E}_{image}^{ref}(\vec{r}) \approx \frac{k}{2\pi f} \pi w_p^2 |\mathcal{E}_{pinhole}(\vec{\delta})| e^{i\varphi_o^{ref}(\vec{r})} e^{-i\chi}$$

where χ is an irrelevant constant. Δ may be calculated from Eq. (6) and the inverted input phase:

$$\Delta(\vec{r}) = \psi(-\vec{r}) + \frac{k}{f}\left(\frac{\delta_z}{2f} r^2 - \delta_x x - \delta_y y\right) + \chi .$$

The maximum visibility of fringes occurs when $|\delta_{image}^{ref}| \approx |\delta_{image}^{trans}|$; using

$$\delta_{image}^{trans}(\vec{r}) = -\tau \delta_{input}(-\vec{r}) ,$$

we see that this implies

$$\tau |\epsilon_o| = \frac{kw_p^2}{2f} |\delta_{pinhole}(\vec{\delta})|$$

or, in terms of intensity and transmission,

$$TI_{input} = \left(\frac{kw_p^2}{2f}\right)^2 I_{pinhole} .$$

II.B. Experimental Illustrations of PDI Operation and Verification of Theory

A commercial PDI[5] was used for testing; it consists of the semitransparent film with pinhole deposited on a mica substrate. Microscopical observation revealed the diameter of the pinhole to be 7 ± 1 μm. A 71 mm diameter, 30 cm focal length spherical lens (of minimized spherical aberration) was used to focus an expanded and collimated He-Ne laser beam onto the pinhole. The incident beam and lens system are subject to some minor phase error. The dark-ring radius is given by Eq. (4)

$$w_{spot}^{DR} = 0.61\, \lambda f / w_o^{HA} \approx 3.3 \text{ μm}$$

where w_o^{HA} is the effective hard-aperture input radius of the beam. Our theory indicates that the reference beam should possess no more than a fraction of a wave of error per input wave based on Eq. (14). Figures 2, 3, and 4 illustrate the interferograms obtained with defocus, null or centered, and tilt
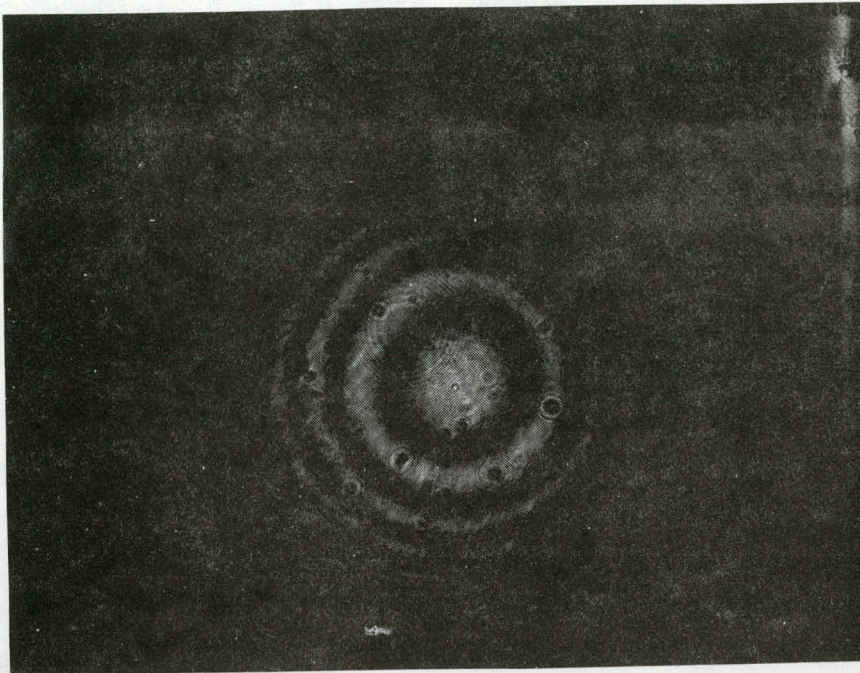
Fig. 2. PDI interferogram showing defocus which corresponds to Eq. (6) of the text having a nonzero δ_z and $\delta_x = \delta_y = 0$.
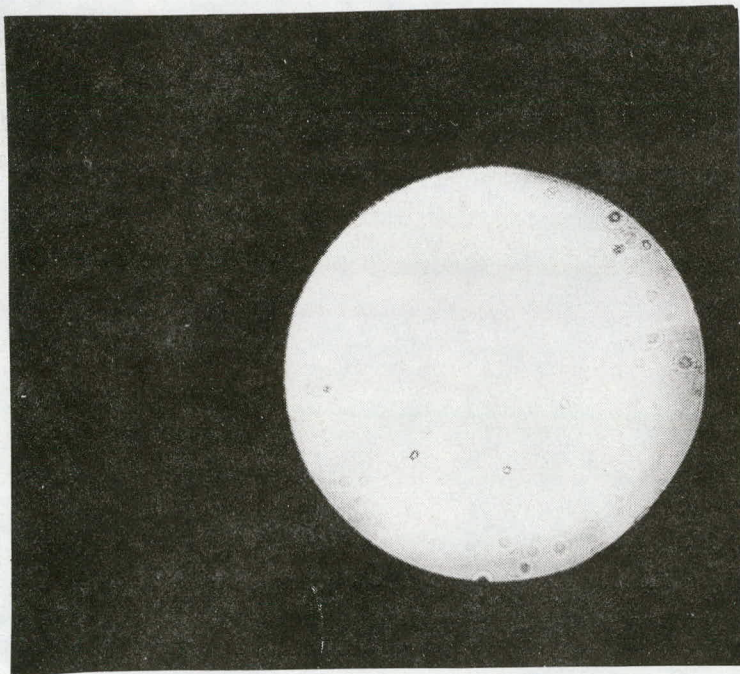
Fig. 3. PDI interferogram with $\delta_x = \delta_y = \delta_z = 0$ and relatively good input beam. This is a null position with all-bright uniform field.
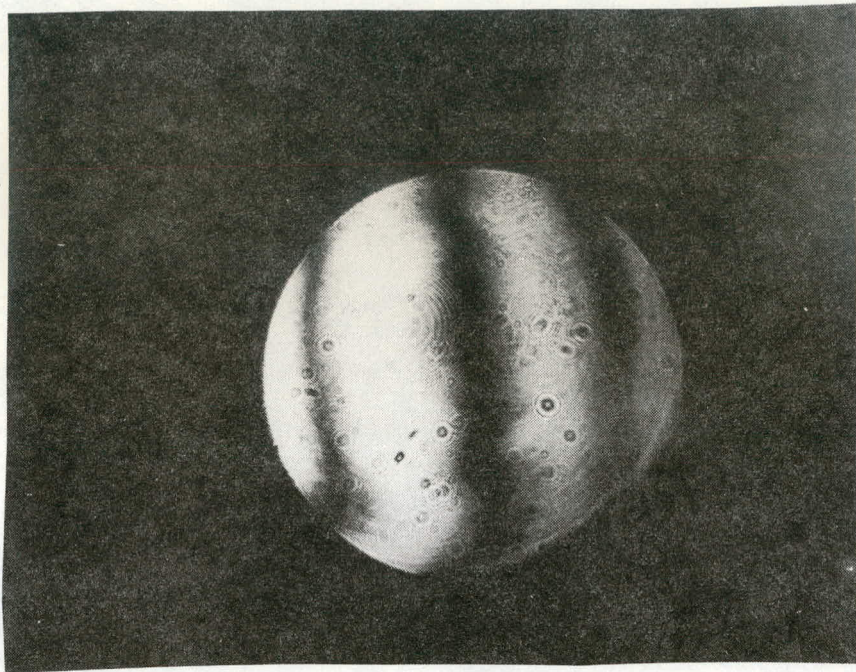
Fig. 4. PDI interferogram with nonzero δ_x or δ_y and $\delta_z = 0$. This is finite tilt with a reference beam phase given by Eq. (6).

Fig. 5. PDI interferogram exhibiting almost pure astigmatism in the input beam. This photo reveals an input beam error and not an adjustment of the interferometer as in Figs. 2, 3, and 4.

23

adjustments. These correspond to: a finite δ_z and $\delta_x = \delta_y = 0$ for

defocus, $\delta_z = \delta_x = \delta_y = 0$ for centered, and $\delta_z = 0$ and finite

δ_x or δ_y for tilt. Figure 5 illustrates classic astigmatism, obtained

by introducing a tilted optical flat into the converging beam.[6]

Spherical aberration is also introduced by the flat, but we could

not observe this distortion since the amount is less than 1/10 wave.

Reversing the 30 cm focal length lens gave a striking abundance of

fringes characteristic of spherical aberrations, on the order of

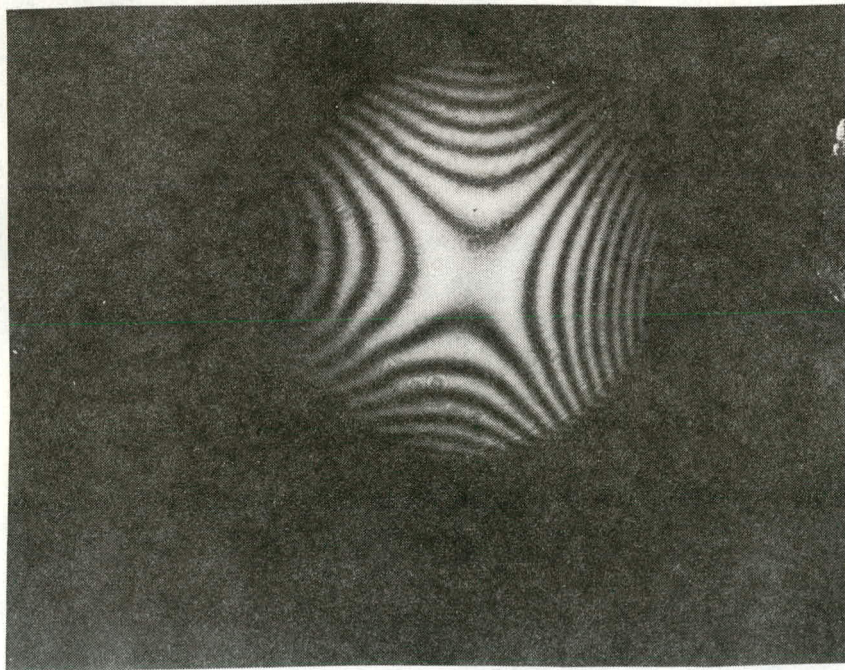50 waves across the field. Since we were limited in stock of good

lenses of small F number, we could not set up a PDI system with a

focus smaller than 7 μm. We could assemble our own pinhole, however,

and found that pinholes considerably larger than 10 μm gave interferograms

of incorrect tilt (as well as other) behavior. Figure 6 shows this

pattern, which is more characteristic of a knife-edge pattern than an

interferometric tilt.

Data[7] presented at the Los Alamos Conference on Optics supports

our theory for pinhole size limitations due to both amplitude and phase

effects. Studies were done involving both computer-generated calculations

and experiments for an input beam possessing one type of aberration

as a function of pinhole diameter. An exact comparison to the data

is difficult to make; however, it is apparent that the phase error

enters the reference beam phase as a high power of w_p/w_{spot}^{DR}, possibly

the fourth. Also, the $w_p/w_{spot}^{DR} = 1$ point has a maximum phase error

on the order of 1/2 wave for input containing one wave of astigmatic

error. If we evaluate Eq. (13) with one wave of astigmatism, i.e.,

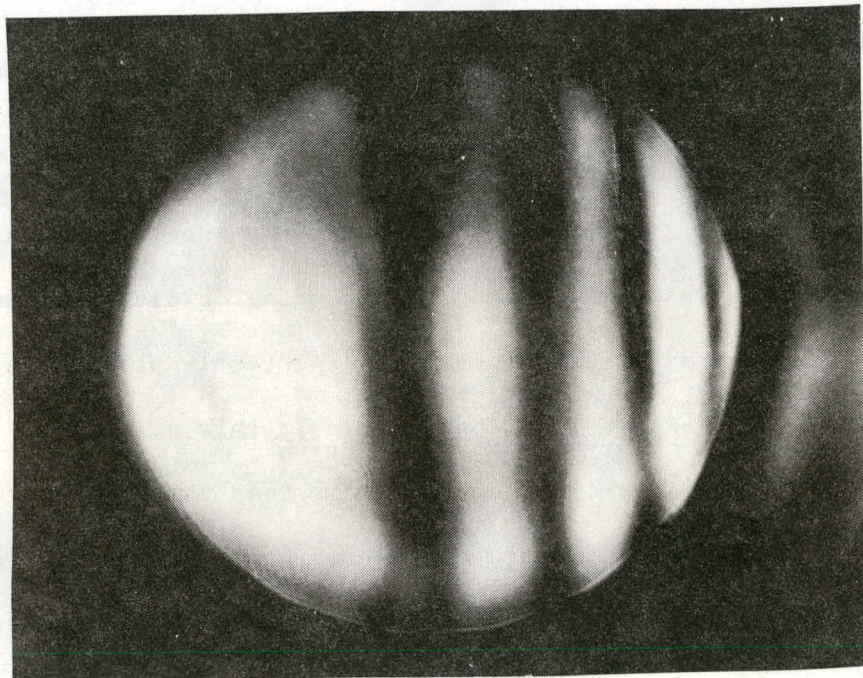$$\bar{\psi} = 2\pi(s/w_o)^2 \cos^2\theta ,$$

Fig. 6. PDI interferogram with much too large of a w_p/w_{spot} ratio. This exhibits a severe reference beam error.

the maximum astigmatic phase error in the reference beam is 4/9 of a wave. Coma is not produced by astigmatism in $\bar{\psi}$. This is probably as close an agreement as we could expect.

III. Optical Properties of Pressurized Windows

Many gas laser systems operate with the pressure considerably above or below the ambient. Speculation always occurs as to the aberrations introduced into the beam by the strained windows, which were presumably flat at zero pressure differential. A theoretical analysis is given in this section of an incident plane beam (all rays collinear) on a pressure-loaded window which is deformed such that the surfaces are concentric spheres or cylinders. It is permissible to treat the surfaces as concentric because of the smallness of Poisson's ratio and also because the positive and negative strains balance at the inner and outer surfaces. We do not treat the general case of a converging or diverging beam incident on a deformed window since even a perfectly plane-parallel optical flat produces spherical aberrations in this case.[6] We also do not consider any piezo-optic effect other than the gross deformation of the refractive body. Data are available[8] for analyzing the strain-optic effect in many crystalline window materials. We do not consider this because of its specific nature and complicated analysis.

We consider the ray-tracing through the curved cross section of a loaded plate shown in Fig. 7. The surface boundaries are concentric circles and a fully three dimensional figure is obtained either by rotation about the optic axis (loaded disk) or by translation normal to the plane of the figure (loaded thin rectangle of cylindrical shape). Let $n_L = n_2/n_1$ and $n_R = n_2/n_3$ denote the appropriate refractive index ratios so that Snell's law for the first (left) and second surfaces reads
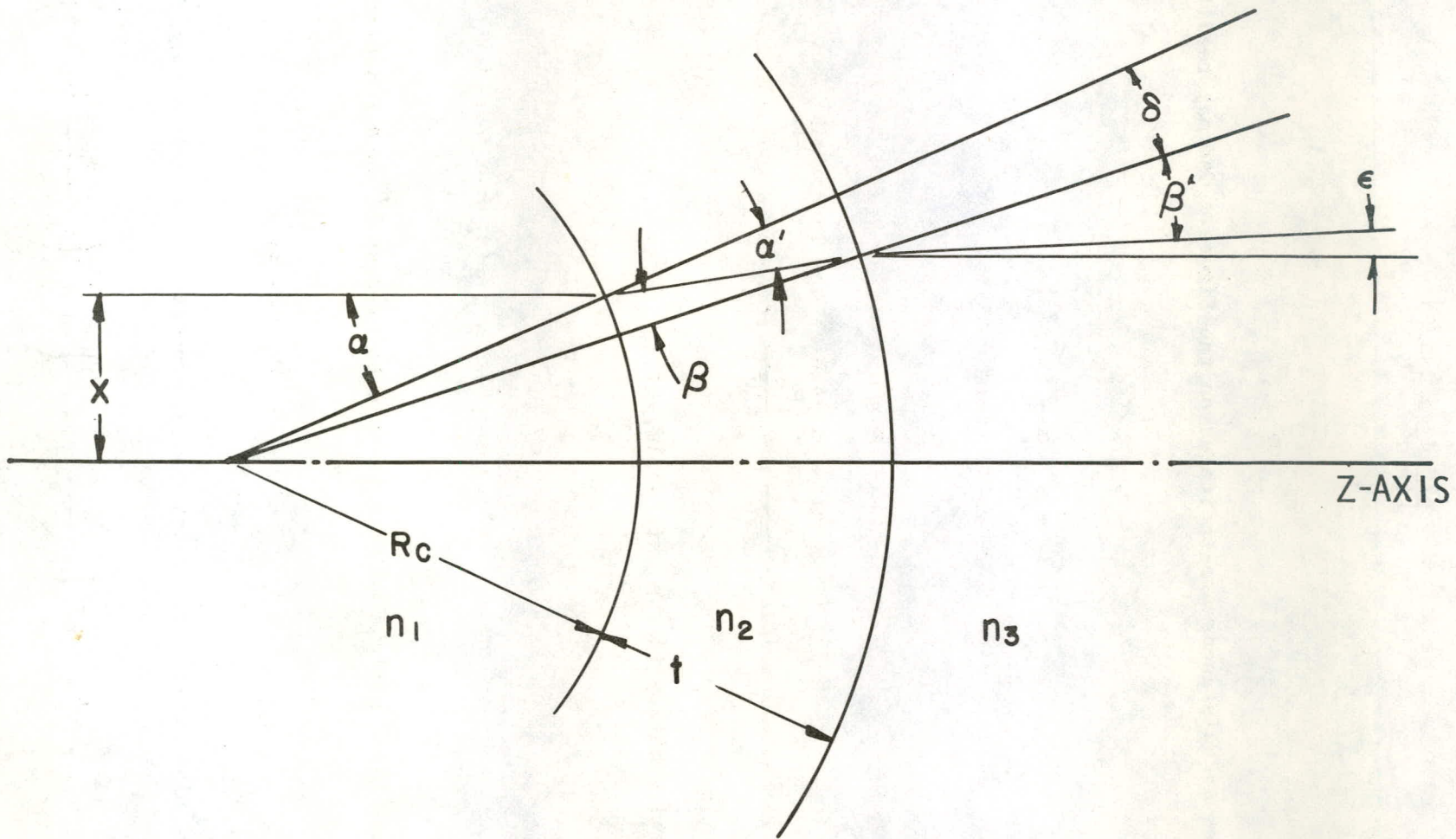
Fig. 7. Ray-tracing diagram used in the theoretical
developmentin Section III for bent windows.

$$\frac{\sin \alpha}{\sin \alpha'} = n_L$$

and

$$\frac{\sin \beta}{\sin \beta'} = \frac{1}{n_R}.$$

All angles and distances are indicated on the figure. One may readily observe

$$\beta = \alpha' - \delta$$

$$\beta' + \epsilon = \alpha - \delta$$

and

$$\sin \alpha = x/R_c$$

$$\frac{R_c + t}{\sin \alpha'} = \frac{R_c}{\sin \beta} \quad .$$

The desired quantity is the exit angle, ϵ:

$$\epsilon = \alpha - \delta - \beta'$$

$$= \alpha - \alpha' + \beta - \beta' .$$

Snell's law for the right surface is used to express β' as a function of β:

$$\epsilon = \alpha - \alpha' + \beta - \sin^{-1}(n_R \sin \beta) .$$

The law of sines relation enables one to express β as a function of α':

$$\epsilon = \alpha - \alpha' + \sin^{-1}\left(\frac{R_c}{R_c + t} \sin \alpha'\right) - \sin^{-1}\left(n_R \frac{R_c}{R_c + t} \sin \alpha'\right) ,$$

and Snell's law for the left surface affords α' as a function of α or x/R_c:

$$\epsilon = \alpha - \sin^{-1}\left(\frac{1}{n_L}\sin\alpha\right) + \sin^{-1}\left(\frac{1}{n_L}\frac{R_c}{R_c + t}\sin\alpha\right)$$

$$- \sin^{-1}\left(\frac{n_R}{n_L}\frac{R_c}{R_c + t}\sin\alpha\right)$$

or,

$$\epsilon = \sin^{-1}\left(\frac{x}{R_c}\right) - \sin^{-1}\left(\frac{1}{n_L}\frac{x}{R_c}\right) + \sin^{-1}\left(\frac{1}{n_L}\frac{x}{R_c + t}\right)$$

$$- \sin^{-1}\left(\frac{n_R}{n_L}\frac{x}{R_c + t}\right) \quad .$$

As a check, one sees that ϵ is zero if t is zero and $n_R = n_L$; that ϵ is zero if x is zero or if R_c is infinite; and that ϵ is zero for $n_L = n_R = 1$. In general R_c/x and R_c/t are much greater than one so that

$$\epsilon \approx \frac{x}{R_c}\frac{n_L - n_R}{n_L} + \frac{x}{R_c}\frac{t}{R_c}\frac{n_R - 1}{n_L}$$

$$= \frac{x}{R_c}\left(1 - \frac{n_1}{n_3}\right) + \frac{x}{R_c}\frac{t}{R_c}\frac{n_2/n_3 - 1}{n_2/n_1} \quad .$$

Suppose ϵ is positive as shown in Fig. 7, then all exit rays appear to emanate from a point which is approximately x/ϵ to the left of the window. In the special case of an incident plane wave, the deformed window acts as a negative lens of focal length f,

$$-\epsilon/x = 1/f = -\left(\frac{1}{R_c}(1 - n_1/n_3) + \frac{t}{R_c^2}\frac{n_2/n_3 - 1}{n_2/n_1}\right) \quad .$$

We now calculate the distortion in a pressure-loaded disk and estimate the maximum distortion that can be obtained without overstressing the material. This distortion will be used to obtain a bound on the number of waves of phase error produced in an incident plane wave. Consider the circular plate of radius a to be supported at the perimeter and loaded uniformly with a pressure differential P. The deflection as a function of radius is given by[9]

$$y(r) = \frac{3P(m^2 - 1)a^2}{8Em^2t^3} \left(\frac{5m + 1}{2(m + 1)} a^2 - \frac{3m + 1}{m + 1} r^2 + \frac{1}{2} \frac{r^4}{a^2} \right)$$

where m is the reciprocal of Poisson's ratio, E is Young's modulus, and t is the thickness. For many glasses, m is in the range of 4 to 6. We pick m = 5 and note that r^4/a^2 can be neglected in comparison to the other terms; this gives the simple form of y(r):

$$y(r) = \frac{3}{4} \frac{Pa^4}{Et^3} \left(1 - (r/a)^2 \right)$$

(20)

$$y_{max} = y(0) = \Delta = \frac{3}{4} \frac{Pa^4}{Et^3} .$$

The maximum stress in the loaded disk occurs at the centers of the surfaces and is given by

$$S = \frac{3a^2P}{8mt^2} (3m + 1)$$

(21)

$$\underset{\substack{\text{glasses} \\ m = 5}}{\approx} \frac{6}{5} P(a/t)^2 \approx P(a/t)^2 .$$

The loaded disk is essentially of the same concentric circular cross section as used in the ray tracing analysis. The radius of curvature is found to be from Eqs. (18) and (20)

$$R_c = \frac{1}{2} \frac{a^2}{\Delta} = \frac{2}{3} \frac{Et^3}{Pa^2} \ . \tag{22}$$

This may now be used in Eqs. (15) and (16) to calculate the contributions to 1/f and that to give the number of waves of error via Eq. (19). Instead of evaluating this for a specific window system, we have found it possible to make a general estimate of the maximum phase error expected.

It is observed that the yield tensile strengths of many materials[8] including glasses[10] are within a factor of two of being one thousandth of their elastic Young's moduli. We use this to set an approximate but useful bound on the maximum deformation of circular windows in normal use:

$$S_{yield} \approx 10^{-3} \ E \ ,$$

$$S < S_{yield} \ ,$$

implying from Eq. (21)

$$P(a/t)^2 < 10^{-3} \ E \ .$$

This can be inserted into the deflection and curvature formulae (Eqs. (20) and (22)) to give

$$\Delta < \frac{3}{4} \ 10^{-3} a^2/t$$

$$R_c > \frac{2}{3} \ 10^3 t \ .$$

Thus, the focal lengths as defined in Eqs. (15) and (16) are bounded,

$$|f_{MEN}| > |\frac{n_L}{n_L - n_R}| \frac{2}{3} 10^3 t$$

$$|f_{WIN}| > |\frac{n_L}{n_R - 1}| \frac{4}{9} 10^6 t \ .$$

The presence of kilotorr pressure differentials on the window will tend to make $n_L - n_R \approx 10^{-3}$ due to gas density effects alone giving the result that $f_{MEN} \approx f_{WIN}$. Typically, $n_L \approx n_R \approx 1.5$ giving

$$|f_{WIN}| > 10^6 t$$

and combined with Eq. (19)

$$N < \frac{a}{2\lambda} \frac{a}{t} 10^{-6} \ .$$

Thus, we have the important conclusion that for windows of nominal diameter to thickness ratio, say six, and micron wavelengths, N is less than 1.5a where the radius a is in meters. It is emphasized that this distortion occurs at a stress near the mechanical yield point of the window. Practical restrictions should ensure that N is never more than one.

An apparatus was set up to test the theory. Rather than using a pressure cell with transmission optics, we attempted to deform glass plates mechanically. Microscope slides and cover glasses are of advantageous length-to-thickness ratio, but breakage occurs frequently before appreciable wave distortion is observed.

The whole problem was circumvented in an acceptable fashion by using a plastic sheet. Figure 8 shows an interferogram of the flat sheet, revealing a

a few waves of optical thickness variation across the approximately 3 cm field. Figure 9 shows the interferogram of the sheet while it is bent into a cylindrical section. The radius of curvature (cylindrical) R_c is 38.1 mm, the sheet thickness t is 0.14 mm, the index of the plastic is 1.67, and the He-Ne wavelength is 0.6328 µm. Thus, up to a distance a = 2 cm from the center of the curvature we should have observed (from Eqs. (15) and (19))

$$N = \frac{a^2}{2\lambda} \frac{n-1}{n} \frac{t}{R_c^2} \approx 12$$

waves of phase distortion. Inspection of Fig. 9 shows that this is almost exactly the case. Thus, by using plastic with a large elastic limit to Young's modulus ratio, we can easily generate many waves of optic distortion and observe the phenomenon with the PDI. The agreement with our theory confirms the optical part of the analysis.

IV. Conclusions

In summary, we have found the PDI a convenient instrument to use. It has been shown to be important that the focusing optics not be casually chosen: the diffraction-limited focal spot should be at least as large as the pinhole to obtain interferograms of near wave accuracy. One disadvantage of the PDI is that the damage threshold of the substrate can be exceeded for short pulses which have sufficient energy to produce film exposure in the interferograms.

A second development is the loaded-window analysis. This shows that gas laser window distortions are negligible under most circumstances (barring birefringent effects in single crystals) because of the strain-stress properties of materials. The PDI was used to confirm the ray-tracing analysis of the phase distortion.
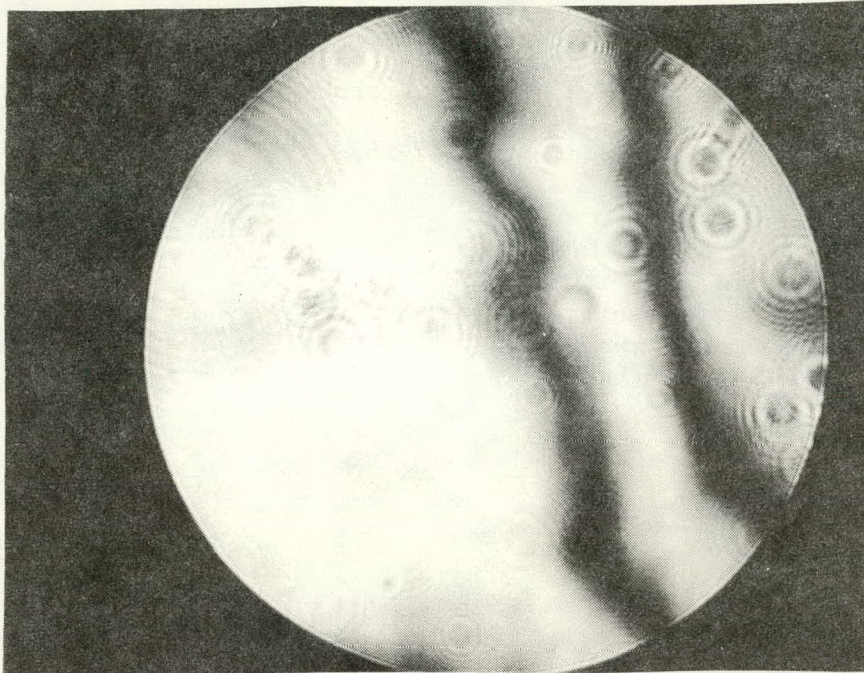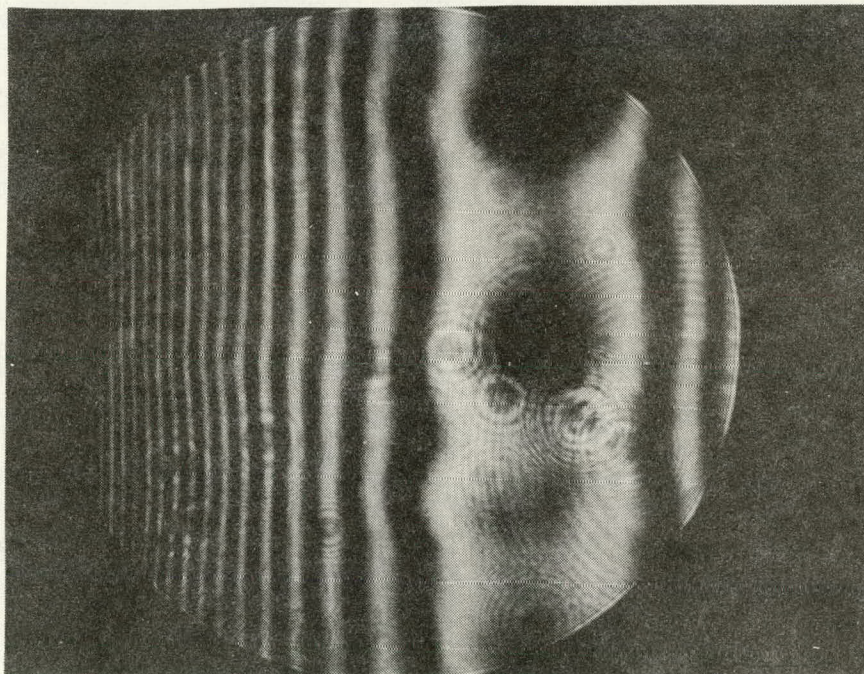
Fig. 8. PDI interferogram of plastic sheet. The sheet is unbent and contains a few waves of nonuniformity in thickness.

2 cm

Fig. 9. PDI interferogram of bent plastic sheet. The center of curvature is off-center in the photo aperture. A two-centimeter scale is indicated below the figure. Discussion is present near the end of Section III.

Acknowledgment

REFERENCES

1. R. N. Smartt and W. H. Steel, "Theory and Application of Point-Diffraction Interferometers," Japan J. Appl. Phys. $\underline{14}$ (1975) Suppl. 14-1.

2. C. Koliopoulos, O. Kwon, R. Shagam, J. C. Wyant, and C. R. Hayslett, "Infrared Point-Diffraction Interferometer," Opt. Lett. $\underline{3}$, 118 (1978).

3. The Rayleigh range of a TEM_{00} Gaussian beam of electric waist w_o is $1/2kw_o^2$. At this distance the waist size will be a factor of $\sqrt{2}$ larger. Any disturbance that is characterized by a transverse dimension w_o will persist until it "diffracts out" at this Rayleigh range.

4. The paraxial propagation formulation is adequate for large or small F number in this analysis since the beam is always being compared to itself over the same path. What errors are introduced by paraxial approximation cancel one another.

5. Available as a Smartt Interferometer from Ealing Corp., South Natick, MA 01760.

6. F. A. Jenkins and H. E. White, "Fundamentals of Optics," (McGraw-Hill, NY, NY 1976) Fourth Edition.

7. J. C. Wyant, "Recent Investigations of Interferometry and Applications to Optical Testing," Proceedings of the Los Alamos Conference on Optics '79, SPIE, Vol. 190, p. 507.

8. American Institute of Physics Handbook, D. E. Gray, Coor. Editor (McGraw-Hill, NY, NY 1972) Third Edition.

9. R. J. Roark, "Formulas for Stress and Strain," (McGraw-Hill, NY, NY 1965) p. 216.

10. The data sheets furnished by several suppliers confirm this as well as the few glasses reported in Ref. 8.

UNLIMITED RELEASE

Distribution:

R. N. Smartt
Sacramento Park Observatory
Sunspot, NM 88349

James C. Wyant
Optical Sciences Center
University of Arizona
Tucson, AZ 85721

Lawrence Livermore National Laboratory
University of California
Library - L-53
P. O. Box 808
Livermore, CA 94550

Los Alamos Scientific Laboratory
Main Library - Mail Stop 362
P. O. Box 1663
Los Alamos, NM 87545

4000	A. Narath
4200	G. Yonas
4210	J. B. Gerardo (2)
4211	E. J. McGuire
4211	M. E. Riley (5)
4212	R. A. Gerber
4212	J. M. Hoffman
4212	J. B. Moreno
4212	E. L. Patterson (5)
4212	G. C. Tisone
4212	J. R. Woodworth
4214	E. D. Jones
4214	P. J. Brannon
4214	C. K. Miller
4216	A. W. Johnson
4216	P. J. Hargis, Jr.
4216	J. P. Hohimer
4218	J. K. Rice
4218	G. A. Fisk
4218	G. N. Hays
4218	W. M. Trott
4240	G. W. Kuswa
4250	T. H. Martin
8266	E. A. Aas
3141	T. L. Werner (5)
3151	W. L. Garner (3) (for DOE/TIC)
3154-3	R. P. Campbell (25)

Org.	Bldg.	Name	Rec'd by*	Org.	Bldg.	Name	Rec'd b

*Recipient must initial on classified documents.